Reconfigurable Intelligent Surface aided Integrated-Navigation-and-Communication in Urban Canyons: A Satellite Selection Approach

Tianwei Hou, *Member, IEEE*, Da Guan, Xin Sun, Anna Li, *Member, IEEE*, Wenqiang Yi, *Member, IEEE*, Yuanwei Liu, *Fellow, IEEE*, Arumugam Nallanathan, *Fellow, IEEE*

***Abstract*—This study investigates the application of a simultaneous transmitting and reflecting reconfigurable intelligent surface (STAR-RIS)-aided medium-Earth-orbit satellite network for providing both global positioning services and communication services in the urban canyons, where the direct satellite-user links are obstructed. Superposition coding and successive interference cancellation techniques are utilized for the integrated navigation and communication (INAC) networks, and the composed navigation and communication signals are reflected or transmitted to ground users or indoor users located in urban canyons. By doing so, it introduces a new challenge: how to select the optimal satellite to simultaneously maximize data rate and ensure high-accuracy positioning. To meet above-mentioned diverse application needs, navigation-oriented INAC and communication-oriented INAC have been developed, each tailored according to distinct power allocation factors. We then proposed two algorithms, namely navigation-prioritized-algorithm and communication-prioritized-algorithm, to improve the navigation or communication performance by selecting the satellite with the optimized position dilution of precision or with the best channel gain. The effectiveness of the proposed STAR-RIS-aided INAC network is quantified by analyzing the positioning error for navigation services and by evaluating communication performance through achievable ergodic rate metrics. Our satellite selection approach indicates that: 1) The positioning services at the urban canyon users can be completed with the aid of STAR-RIS. 2) Additionally, it is observed that while a single STAR-RIS array can extend the navigational link, it fails to serve users in indoor scenarios, highlighting a limitation in the current system design.**

This work was supported in part by the Fundamental Research Funds for the Central Universities under Grant 2023JBZY012 and 2024JBMC014, in part by the National Natural Science Foundation for Young Scientists of China under Grant 62201028, in part by Young Elite Scientists Sponsorship Program by CAST under Grant 2022QNRC001, in part by the Beijing Natural Science Foundation L232041, in part by EPSRC grant numbers to acknowledge are EP/W004100/1, EP/W034786/1, EP/Y037243/1 and EP/W026813/1. (Corresponding author: Anna Li.)

T. Hou is with the School of Electronic and Information Engineering, Beijing Jiaotong University, Beijing 100044, China, and also with the School of Electronic Engineering and Computer Science, Queen Mary University of London, London E1 4NS, U.K. (email: twhou@bjtu.edu.cn).

Da Guan and Xin Sun are with the School of Electronic and Information Engineering, Beijing Jiaotong University, Beijing 100044, China(e-mail:23111014@bjtu.edu.cn; xsun@bjtu.edu.cn).

Anna Li is with the School of Computing and Communications, Lancaster University, Lancaster LA1 4WA, U.K. (e-mail: a.li16@lancaster.ac.uk).

Wenqiang Yi is with the School of Computer Science and Electronic Engineering, University of Essex, Colchester CO4 3SQ, U.K. (email: w.yi@essex.ac.uk).

Yuanwei Liu is with the Department of Electrical and Electronic Engineering, The University of Hong Kong, Hong Kong (e-mail: yuanwei@hku.hk).

A. Nallanathan is with the School of Electronic Engineering and Computer Science, Queen Mary University of London, London, U.K. and also with the Department of Electronic Engineering, Kyung Hee University, Yongin-si, Gyeonggi-do 17104, Korea (e-mail: a.nallanathan@qmul.ac.uk).

***Index Terms*—Integrated-navigation-and-communication (INAC), indoor positioning, superposition coding, STAR-RIS, urban canyons.**

I. Introduction

The global navigation satellite system (GNSS), renowned for providing robust all-weather positioning and precise time services, plays a critical role in a myriad of contemporary applications [1]–[3]. GNSS is integral to various consumer devices, providing centimeter-level positioning accuracies through GNSS carrier phase measurements [4]. By 2020, the standards for positioning accuracy have evolved from the 10 cm 2-dimensional requirement in fifth-generation (5G) systems to an enhanced 1 cm accuracy in 3-dimensional (3D) space for next-generation navigation systems. [5]. However, the coverage of GNSS faces challenges when serving areas without direct line-of-sight (LoS) links, such as urban canyons, where the street is flanked by high buildings on both sides creating a canyon-like environment [6], [7].

In GNSS, navigation services are mainly deployed at the medium-earth-orbit (MEO) satellites. Given that MEO navigation satellites are situated at altitudes exceeding 20,000 km, the signal power received in open scenarios is approximately -130 dBm [8]. In [9], it is indicated that the received signal power is further attenuated by -20 dB in the urban canyons. Additionally, satellite signals reflected from different surfaces in the urban canyon further complicate the evaluation of the pseudo-range via time of flight. To solve the lack of LoS issues in the urban canyons, existing works have tried from three directions: 1) additional information aided navigation technique; 2) Rayleigh fading channel aided navigation technique; 3) Mega constellation aided navigation technique. For 1), the use of supplementary information, such as 3D maps, also aids navigation when satellite signals are sparse [10]. For 2), in order to provide navigation services in non-LoS (NLoS) cases, the indoor navigation technique based on the Rayleigh fading channel has been proposed, where the indoor distance is evaluated by the multi-path fading with the aid of estimator-correction [11]. The channel statistic can also be predicted in the urban canyons for proving inertial navigation services [12]. For 3), In [13], since more low-Earth-orbit (LEO) satellites are located at the high pitch angle regimes than that of the MEO satellite in the deep urban canyons, which indicates that the Mega LEO constellations offer better geometric dilution of precision than that of the MEO constellations. However, these approaches, such as distributed beamforming [14], do

not create extended LoS links between satellites and users in the urban canyons.

In order to solve the above mentioned issues of the navigation systems, reconfigurable intelligent surface (RIS) emerges as a promising solution. RISs are able to reshape the electromagnetic propagation environment into a controlled format and alter the phase of incoming signals [15], [16]. In a word, RISs are able to create new LoS links via reflecting or refracting signals [17]. More specifically, a RIS array consists of numerous passive reflective intelligent surface elements, each containing a reflector layer that can independently induce a phase shift in the electromagnetic wave [18]–[20]. By doing so, RISs are capable of enhancing the signal power to different wireless applications [21]–[25]. In [26], the performance gain of RIS-aided networks was analyzed with the assistance of unmanned aerial vehicles. The RIS-aided 5G networks was proposed, revealing improvements in signal quality and coverage areas [27]. An energy efficiency optimization algorithm was proposed in the RIS-aided multi-user networks, where the phase shift of the RIS array was designed [28]. In [29], the applications of GNSS have been explored, where RIS stands as an potential solution. When the RIS array is deployed on the building surfaces, the LoS links between satellite and blocked users in urban canyons can be extended [30]. By deploying RIS into the unmanned aerial vehicle, navigation and communications in 3D can be realized [31], [32]. Traditional RIS implementations have been limited by the requirement that receivers must be located on the same side as the transmitters. In order to release the above constraint of RIS-aided networks, the concept of simultaneous transmitting and reflecting RIS (STAR-RIS) was proposed in [33]–[35]. Furthermore, the signal model based on dual-sided STAR-RIS was provided in [36], where the STAR-RIS can achieve full diversity order on both sides of the surface and extend the coverage significantly [34], which has huge development potentials for wireless communication networks. Utilizing the advanced STAR-RIS technique holds the potential to revolutionize navigation accuracy in urban canyons, marking a significant advancement over current satellite navigation solutions [37]. The application of RIS in indoor positioning has been analysed in [38], where the Sidelink technique is employed to provide positioning services.

Recently, the integrated navigation and communication (INAC) technique is expected to be considered to meet future requirements of satellite networks. Given their relatively lower altitude, LEO satellites are well-suited for communication services but fall short in providing precise navigation due to inadequate dilution of precision. Hence, INAC systems are more favorably deployed on MEO satellites. High-altitude platforms have been proposed for simultaneously delivering cellular communication and navigation services, using communication channels for navigation message transmission [39]. Moreover, the integration of communication and navigation services via near-space platforms has shown distinct advantages, particularly in wide-range monitoring applications, outperforming traditional satellite and airborne networks [40]. A crossover multiple-way ranging protocol for device-to-device positioning measure in 5G communication networks was proposed without increasing resource demands, compared to traditional two-way ranging protocols [41]. As mentioned above, the conventional INAC network usually relies on time-division-multiple-access techniques, where navigation and communication signals are separated by time resource blocks, potentially compromising navigation performance [42]. Therefore, obtaining a novel solution that can simultaneously provide communication and navigation services becomes the primary goal. Non-orthogonal multiple access (NOMA) is increasingly recognized as an effective technique in wireless communications, facilitating access for numerous users [43]–[45]. The NOMA technique can serve users at different quality-of-service requirements, which is natural to implement the navigation and communication services in the same time/frequency/code resource blocks by NOMA technique for the INAC networks [46]. The RIS-NOMA-aided INAC network was initially explored in [47], which examined both communication-oriented and navigation-oriented INAC. Key performance indicators were evaluated to determine the effectiveness of INAC networks, e.g., outage probability, channel capacity, and navigation accuracy. The application of RIS-aided LEO satellite beam-tracking has been explored in [48], where the positions of users are evaluated by the Riemannian manifold algorithm.

Based on the previous contributions [46], [47], where the RIS-aided satellite navigation has been proven to be feasible, the STAR-RIS-NOMA-aided INAC in the urban canyons has not been studied extensively, resulting in the following three additional challenges: i) To overcome the requirement of LoS links in the conventional GNSS, can STAR-RIS provide additional links for urban canyon and indoor scenarios? ii) Since multiple satellites are located in orbit simultaneously, the satellite selection algorithm providing the optimized positioning accuracy and communication performance is still expected. iii) The optimized power allocation of communication-oriented (CO)-INAC and navigation-oriented (NO)-INAC is still unknown. Therefore, this article aims at integrating STAR-RIS and NOMA techniques into the INAC networks, where the high data rate requirement of communications and the high positioning accuracy requirement of navigation in urban canyons can be both satisfied.

Based on the above background, our main contributions are concluded as follows:

- We introduce a pioneering STAR-RIS-NOMA-assisted MEO satellite INAC network specifically designed for urban canyons. By utilizing the superposition coding (SC) and successive interference cancellation (SIC) techniques, navigation and communication signals are efficiently fused in the same time/frequency/code resource blocks. We propose both CO-INAC and NO-INAC cases based on the power allocation factors.
- In order to provide the optimized performance of navigation, we first formulate the positioning equations of the proposed STAR-RIS assisted INAC network. Then, the penalty-based navigation-prioritized-algorithm (NPA) is proposed to select the satellite with the minimized position dilution of precision (PDoP). By doing so, the proposed NPA is capable of providing the optimized positioning error for both outdoor and indoor users.

- On the contrary, another communication-prioritized-algorithm (CPA) has been proposed to enhance the communication performance. With the designed passive beamforming at STAR-RIS, the achievable ergodic rates of both outdoor and indoor users are optimized, which demonstrate the feasibility of the proposed STAR-RIS-assisted INAC networks.
- The simulation results demonstrate that: 1) the proposed STAR-RIS-NOMA-assisted INAC systems can provide revolutionary solutions in the urban canyon and indoor scenarios; 2) The indoor users suffer higher positioning error than the outdoor users, where the positioning error of the indoor users mainly depends on the distance between the STAR-RIS and users; 3) The nearest INAC satellite is expected to enhance the communication performance, which may not proper for the navigation services.

A. Organization

In Section II, the system model, signal model, and urban canyons are proposed. Section III describes the positioning principles of this article. In Section IV, we introduce our novel objective functions and passive beamforming at STAR-RIS. The simulation analysis of the proposed STAR-RIS-NOMA-assisted INAC networks in terms of positioning accuracy and achievable ergodic rate are verified in Section IV. Finally, section V concludes this paper.

II. System Model

This article examines a new STAR-RIS-NOMA-assisted INAC network as shown in Fig. 1. M and N denote the number of transmitting antennas (TAs) at the satellite and number of STAR-RIS elements, respectively.

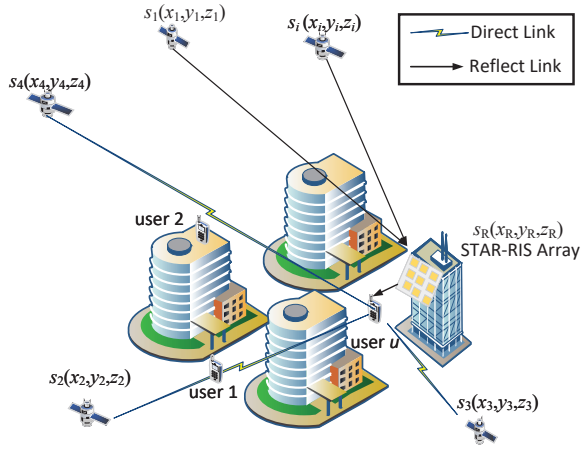

Fig. 1. STAR-RIS-NOMA-assisted INAC networks.

More specifically, Fig. 2 illustrates both the outdoor and indoor scenarios adopted in this article. In Fig. 2(a), the outdoor user receives both direct and reflected signals from multiple satellites via a STAR-RIS array deployed on the building facade, where the direct path may be blocked by obstacles. In Fig. 2(b), the indoor user relies on the reflected signals provided by the STAR-RIS array to overcome severe wall and roof penetration loss.

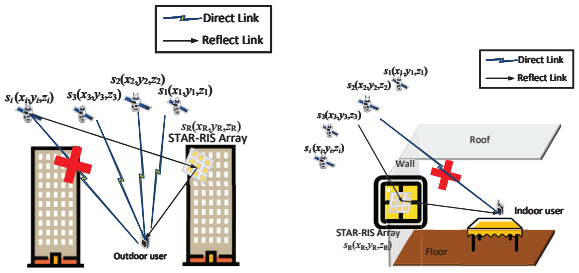

(a) Outdoor scenarios. (b) Indoor scenarios.

Fig. 2. Illustration of outdoor and indoor scenarios.

A. Channel Model

The network contains I satellites, U users, and a STAR-RIS array. We first define the i-th satellite as s_i. Then, we pay our attention to the large-scale fading channels of $s_i - user_u$, which can be expressed as

$$L_{iu} = G_T \left(\frac{\lambda}{4\pi r_{\tau,iu}} \right)^2, \tag{1}$$

where G_T denote the transmit antenna gain. λ denotes the signal wavelength. $r_{\tau,iu}$ is the distance of satellite i and user u.

Note that in the urban canyons, the direct link between satellite and ground users may not exist. Therefore, the STAR-RISs can provide supplementary links between satellite and ground users, and the large scale fading channels of $s_i - STAR - RIS - user_u$ can be given by:

$$L_{Riu} = G_T G_R \left(\frac{\lambda}{4\pi r_{\tau iR}} \right)^2 \left(\frac{\lambda}{4\pi r_{\tau Ru}} \right)^2, \tag{2}$$

where $r_{\tau iR}$ and $r_{\tau Ru}$ respectively represent the distance of $s_i - STAR - RIS$ and $STAR - RIS - user_u$ links, G_R denotes the receive antenna gain.

We then define the small-scale fading channel gain of $s_i - user_u$ link, h_{iu}, which follows the shadowed Rician fading. Although M TAs are deployed, based on the fixed beamforming strategy adopted in GNSS and Beidou system, the multi-antenna gain can be considered as a single variable. Therefore, the small-scale fading vector $\mathbf{h}_u$ received by user u can be expressed as

$$\mathbf{h}_u = \begin{bmatrix} h_{1u} \\ h_{2u} \\ \vdots \\ h_{Iu} \end{bmatrix}, \tag{3}$$

where $\mathbf{h}_u$ is a $(I \times 1)$-element vector. Note that when the direct link between satellite i and user u does not exist, the corresponded row in (3) can be simply set to 0.

Based on the insight of [49], the probability density function and cumulative density function of shadowed Rician fading in

$s_i - user_u$ link are formulated as follows:

$$f_{|h|^2}(x) = \frac{1}{2b}\left(\frac{2bm}{2bm+\Omega}\right)^m e^{-\frac{x}{2b}} \times {}_1F_1\left(m;1;\frac{x\Omega}{2b(2bm+\Omega)}\right), \tag{4}$$

and

$$F_{|h|^2}(x) = K\sum_{n=0}^{\infty}\frac{(m)_n\delta^n(2b)^{1+n}}{(n!)^2}\gamma\left(1+n,\frac{x}{2b}\right), \tag{5}$$

respectively, where $\gamma(a,x) = \int_0^x t^{a-1}e^{-t}dt$ represents the lower incomplete Gamma function, $(m)_k = \Gamma(m+k)/\Gamma(m)$ represents the Pochhammer symbol, $\Gamma(m)$ represents the Gamma function, $\delta = \frac{\Omega}{2b(2bm+\Omega)}$, and $K = \left(\frac{2bm}{2bm+\Omega}\right)^m \frac{1}{2b}$. Ω and $2b$ represent the average power of LoS component and multipath component, respectively. m is the Nakagami-m parameter ranging from zero to infinite. ${}_1F_1(a;b;x)$ denotes the confluent hypergeometric function.

The small-scale channel matrix of $s_i - STAR-RIS$ links is expressed as

$$\mathbf{h}_{Ri} = \begin{bmatrix} h_{R,i1} \\ h_{R,i2} \\ \vdots \\ h_{R,iN} \end{bmatrix}, \tag{6}$$

where $h_{R,in}$ denotes the small-scale fading gain between satellite i and the n-th STAR-RIS element, which follows shadowed Rician fading gains.

Similarly, the small-scale channel matrix of $STAR-RIS-user_u$ is given by:

$$\mathbf{g}_u = \begin{bmatrix} g_{R,1u} & \cdots & g_{R,Nu} \end{bmatrix}, \tag{7}$$

where $g_{R,nu}$ denotes the small-scale channel gain between the n-th STAR-RIS element and user u, which follows the Rician fading channel gains.

To conclude, the channel models for the satellite–user, satellite–RIS, and RIS–user links can be summarized as follows:

- Satellite-user link: Shadowed Rician fading channels.
- Satellite-RIS link: Shadowed Rician fading channels.
- RIS-user link: Rician fading channels.

For simplicity, it is assumed that the satellite-user, satellite-RIS, and RIS-user links share identical fading parameters.

The STAR-RIS adopts both the reflective and transmit layers, thus we define the reflection and transmission matrix as:

$$\mathbf{\Psi}_R = \mathrm{diag}\begin{bmatrix} \beta_{1,R}\phi_{1,R} & \beta_{2,R}\phi_{2,R} & \cdots & \beta_{N,R}\phi_{N,R} \end{bmatrix}, \tag{8}$$

and

$$\mathbf{\Psi}_T = \mathrm{diag}\begin{bmatrix} \beta_{1,T}\phi_{1,T} & \beta_{2,T}\phi_{2,T} & \cdots & \beta_{N,T}\phi_{N,T} \end{bmatrix}, \tag{9}$$

where $j = \sqrt{-1}$, $\phi_{n,R} = \exp(j\theta_{n,R})$ and $\phi_{n,T} = \exp(j\theta_{n,T})$ respectively represent the phase shift of the reflected and transmitted signals of STAR-RIS element n. $0 \le \theta_{n,R} < 2\pi$, $0 \le \theta_{n,T} < 2\pi$. $0 < \beta_{n,R} \le 1$ and $0 < \beta_{n,T} \le 1$ denote the reflection amplitude coefficient and transmission amplitude coefficient of the n-th STAR-RIS element with $\beta_{n,R}^2 + \beta_{n,T}^2 = 1$, respectively.

Regarding ground user u located in the urban canyons, without loss of generality, it is assumed that the number of visible satellites for user u is defined as $I_v, I_v \in I$. In addition, some satellites are invisible for user u, which are defined by a set of $I_n, I_n \in I$. Hence, if user u is located at the reflection space of STAR-RIS, the received signals of user u can be expressed as

$$y_{u,R}(t) = \underbrace{\sum_{i=1,i\in I_n}^{I}\left(\mathbf{g}_u\mathbf{\Psi}_R\mathbf{h}_{Ri}\right)\sqrt{L_{Riu}p_i}s_i(t)}_{\text{Reflected Signals}} + \underbrace{\sum_{i=1,i\in I_v}^{I}h_{iu}\sqrt{L_{iu}p_i}s_i(t)}_{\text{Directed Signals}} + n_0, \tag{10}$$

where n_0 denotes the additive white Gaussian noise (AWGN), $s_i(t)$ denotes the information of the i-th satellite. p_i represents the transmit power of satellites i.

On the other hand, if user u is located in the indoor scenarios, the transmitted signals can be expressed as

$$y_{u,T}(t) = \underbrace{\sum_{i=1,i\in I_n}^{I}\left(\mathbf{g}_u\mathbf{\Psi}_T\mathbf{h}_{Ri}\right)\sqrt{L_{Riu}p_i}s_i(t)}_{\text{Transmitted Signals}} + n_0. \tag{11}$$

B. Signal Model

Due to the fact that the code division technique is deployed in satellite navigation, the users can separate the information of different satellites. Therefore, we simply assume that one INAC satellite is deployed. The SC and SIC techniques are employed at the INAC satellite and ground users to detect the composite signals, respectively. Then, the INAC satellite sends the following signal:

$$s_i(t) = \omega_N s_{i,N}(t) + \omega_C s_{i,C}(t), \tag{12}$$

where ω_N and ω_C represent the power allocation factors of navigation and communication signals, respectively. $s_{i,N}(t)$ and $s_{i,C}(t)$ denote navigation and communication signals, respectively. Under the NOMA protocol, the power allocation factors are constrained such that $\omega_N^2 + \omega_C^2 = 1$. As can be seen from (12), two potential cases with different power allocation factors, NO-INAC and CO-INAC, can be investigated.

- NO-INAC Case: More power is allocated to the navigation signals in the NO-INAC case, where the communication signal must be decoded after the navigation signal is recovered. Fortunately, since navigation typically requires a lower data rate than communication, NO-INAC is more suitable for high transmit power scenarios.
- CO-INAC Case: On the contrary, when the transmit power is insufficient, and the minimum navigation requirement must be met, more power is allocated to communication signals, namely CO-INAC case.

1) NO-INAC Case: It is assumed that the power allocation factors satisfy

$$\omega_C > \omega_N. \tag{13}$$

In this scenario, the INAC user initially decodes the communication signal, treating the navigation signal as interference, and the signal-to-interference-plus-noise ratio (SINR) can be expressed as follows:

$$SINR_C^{NO} = \frac{\left|\tilde{h}_u\right|^2 \omega_C^2 p_i}{\left|\tilde{h}_u\right|^2 \omega_N^2 p_i + \sigma^2}, \tag{14}$$

where $\left|\tilde{h}_u\right|^2$ denotes the channel gain of user u, σ^2 represents the power of AWGN. In this article, there are two possible scenarios. On the one hand, when both the direct link and reflect link exist, the effective channel gain of the outdoor users can be expressed as

$$\left|\tilde{h}_u\right|^2 = \left|\tilde{h}_{u,dir}\right|^2 = \left|\mathbf{g}_u \mathbf{\Psi}_R \mathbf{h}_{Ri} \sqrt{L_{Riu}} + h_{iu} \sqrt{L_{iu}}\right|^2. \tag{15}$$

On the other hand, when the direct link does not exist, the effective channel gain of the indoor users is given by

$$\left|\tilde{h}_u\right|^2 = \left|\tilde{h}_{u,ind}\right|^2 = \left|\mathbf{g}_u \mathbf{\Psi}_R \mathbf{h}_{Ri} \sqrt{L_{Riu}}\right|^2. \tag{16}$$

After the communication signals are subtracted from the received signals, the navigation signals can be detected, then the SINR of navigation signals is given by

$$SINR_N^{NO} = \frac{\left|\tilde{h}_u\right|^2 \omega_N^2 p_i}{\sigma^2}. \tag{17}$$

Therefore, in the NO-INAC case, the achievable navigation rate and communication rate of the INAC user can be given by

$$R_N^{NO} = \log_2\left(1 + SINR_N^{NO}\right), \tag{18}$$

and

$$R_C^{NO} = \log_2\left(1 + SINR_C^{NO}\right), \tag{19}$$

respectively.

2) CO-INAC Case: In the CO-INAC scenarios, we prioritize communication services, leading to the condition where ω_N and ω_C satisfy $\omega_C < \omega_N$. Thus, following the NOMA protocol, navigation signals should be decoded prior to communication signals. Consequently, the SINR for decoding navigation signals can be formulated as:

$$SINR_N^{CO} = \frac{\left|\tilde{h}_u\right|^2 \omega_N^2 p_i}{\left|\tilde{h}_u\right|^2 \omega_C^2 p_i + \sigma^2}. \tag{20}$$

After the navigation signals are deleted from the received signal, the communication signals can be obtained with the following SINR

$$SINR_C^{CO} = \frac{\left|\tilde{h}_u\right|^2 \omega_C^2 p_i}{\sigma^2}. \tag{21}$$

Therefore, the achievable rates of communication and navigation of users in the CO-INAC cases are given by

$$R_C^{CO} = \log_2\left(1 + SINR_C^{CO}\right), \tag{22}$$

and

$$R_N^{CO} = \log_2\left(1 + SINR_N^{CO}\right), \tag{23}$$

respectively.

III. Problem Formulation

A. Geometric Positioning Principle

In this subsection, we first describe the geometric positioning principle. The locations of user u, satellite s_i and STAR-RIS array are specified as (x_u, y_u, z_u), (x_i, y_i, z_i) and (x_R, y_R, z_R), respectively. The GNSS system utilizes a highly accurate clock system that precisely records the transmission time t_{si} when satellite s_i sends a message frame. Similarly, user u records the reception time t_{ru} of the message. The distance $r_{\tau,iu}$ between satellite s_i and user u is then calculated using the speed of light. Likewise, by employing both the speed of light and the transmission times, the combined distance through the STAR-RIS array, expressed as $r_{\tau iR} + r_{\tau Ru}$, is also computed.

When a direct link between satellite s_i and the ground user is established, the positioning equation for satellite s_i can be derived from the Euclidean distance as follows:

$$r_{\tau,iu} = \sqrt{(x_i - x_u)^2 + (y_i - y_u)^2 + (z_i - z_u)^2}. \tag{24}$$

B. Pseudo-Range Positioning

In practical applications, the pseudo-range primarily comprises clock error and atmospheric delay error. It is assumed that satellite s_i transmits a navigation message at its clock time t_{si}, and user u receives this message at their local time t_{ru}. Thus, the estimated distance of $s_i - user_u$ link can be expressed as:

$$\rho_{t,iu} = c(t_{ru} - t_{si}). \tag{25}$$

Given that the satellite clock is not perfectly synchronized with the standard time, it is assumed that the clock error between satellite s_i and the standard clock to be Δt_{si}, and the clock error between user u's clock and the standard clock to be Δt_{ru}. Additionally, the delays caused by the ionosphere and troposphere are represented as I_i and T_i, respectively. Other systematic errors are $\Delta\varepsilon_i$. Considering all the above factors, the actual distance of $s_i - user_u$ can be further transformed into:

$$r_{\tau,iu} = \rho_{t,iu} - c(\Delta t_{ru} - \Delta t_{si} + I_i + T_i + \Delta\varepsilon_i), \tag{26}$$

where Δt_{si} can be obtained by the navigation messages. Thus, the pseudo-range can be simplified to

$$\rho_{ci} = \rho_{t,iu} + c(\Delta t_{si} - I_i - T_i). \tag{27}$$

By doing so, the actual distance of $s_i - user_u$ can be simplified to

$$r_{\tau,iu} = \rho_{ci} - c\Delta t_r, \tag{28}$$

where Δt_r represents the remained clock error with $\Delta t_r = \Delta t_{ru} + \Delta\varepsilon_i$.

Based on (24) to (28), the goal of this article is to calculate four unknowns x_u, y_u, z_u, and Δt_r. Thus, we assume that user u receives several signals from satellite, which are given by

$$\begin{aligned}\sqrt{(x_1-x_u)^2+(y_1-y_u)^2+(z_1-z_u)^2}&=\rho_{c1}-c\Delta t_r,\\ &\vdots\\ \sqrt{(x_i-x_u)^2+(y_i-y_u)^2+(z_i-z_u)^2}&=\rho_{ci}-c\Delta t_r.\end{aligned} \tag{29}$$

Note that in practice, at least four satellites are required for navigation positioning. However, in the urban canyons, the direct link between satellite and user may be blocked. Fortunately, the STAR-RIS is able to provide extended LoS path between satellite and user. Therefore, the positioning equation between satellite v and user u through STAR-RIS is given by

$$\begin{aligned}&r_{\tau,vR}+\sqrt{(x_R-x_u)^2+(y_R-y_u)^2+(z_R-z_u)^2}\\ &=\rho_{cv}-c\Delta t_r,\end{aligned} \tag{30}$$

where ρ_{cv} represents the modified pseudo-range between the v-th satellite to user u via STAR-RIS. The Euclidean distance of the v-th satellite to STAR-RIS is defined by $r_{\tau,vR}$ as:

$$r_{\tau,vR}=\sqrt{(x_v-x_R)^2+(y_v-y_R)^2+(z_v-z_R)^2}, \tag{31}$$

where x_v, y_v and z_v represent the coordinates of satellite v.

We can re-formulate multiple positioning equations as follows:

$$\begin{aligned}\rho_{c1}(\mathbf{x}_r)&=\sqrt{(x_1-x_u)^2+(y_1-y_u)^2+(z_1-z_u)^2}+c\Delta t_r,\\ &\vdots\\ \rho_{ci}(\mathbf{x}_r)&=\sqrt{(x_i-x_u)^2+(y_i-y_u)^2+(z_i-z_u)^2}+c\Delta t_r,\\ \rho_{cv}(\mathbf{x}_r)&=r_{\tau,vR}+\sqrt{(x_R-x_u)^2+(y_R-y_u)^2+(z_R-z_u)^2}\\ &\quad+c\Delta t_r,\end{aligned} \tag{32}$$

where $\mathbf{x}_r=[x_u,y_u,z_u,\Delta t_r]^T$, $\rho_{ci}(\mathbf{x}_r)$ represent the corrected pseudo-range of s_i-user_u link.

We adopt the least squares method (LSM) algorithm to evaluate the position of users, and the state equation is given by

$$\mathbf{b}=\mathbf{A}d\mathbf{x}+\mathbf{N}_0, \tag{33}$$

where $\mathbf{x}$ denotes a vector with 4×1 unknowns, $\mathbf{b}$ represents an $(i+v)\times1$ vector. $\mathbf{N}_0$ represents the AWGN with vector with 4×1 dimension. $\mathbf{A}$ is a $(i+v)\times4$ matrix, which can be calculated from the navigation messages as follows:

$$\mathbf{A}=\begin{bmatrix}\mathbf{u}_1 & \cdots & \mathbf{u}_i & \mathbf{u}_v\end{bmatrix}^T, \tag{34}$$

where $\mathbf{u}_i=\begin{bmatrix}\frac{x_i-x_{u0}}{r_i(\mathbf{x}_{r0})} & \frac{y_i-y_{u0}}{r_i(\mathbf{x}_{r0})} & \frac{z_i-z_{u0}}{r_i(\mathbf{x}_{r0})} & c\end{bmatrix}$, and $d\mathbf{x}_0=\begin{bmatrix}x_u-x_{u0}\\ y_u-y_{u0}\\ z_u-z_{u0}\\ (\Delta t_r-\Delta t_{r0})\end{bmatrix}$.

The cost function $\mathbf{P}(\mathbf{x})$ is defined as

$$\begin{aligned}\mathbf{P}(\mathbf{x})&=(\mathbf{A}\mathbf{x}-\mathbf{b})^T(\mathbf{A}\mathbf{x}-\mathbf{b})\\ &=\mathbf{x}^{\mathrm{T}}\mathbf{A}^{\mathrm{T}}\mathbf{A}\mathbf{x}-2\mathbf{x}^{\mathrm{T}}\mathbf{A}^{\mathrm{T}}\mathbf{b}+\mathbf{b}^{\mathrm{T}}\mathbf{b},\end{aligned} \tag{35}$$

where $\mathbf{P}(\mathbf{x})$ is the sum square error. The goal of LSM is to minimize the sum of squared errors by differentiating $\mathbf{P}(\mathbf{x})$ with respect to x, we can derive:

$$\frac{\partial\mathbf{P}(\mathbf{x})}{\partial\mathbf{x}}=2\mathbf{A}^{\mathrm{T}}\mathbf{A}\mathbf{x}-2\mathbf{A}^{\mathrm{T}}\mathbf{b}. \tag{36}$$

The extreme point of the cost function is

$$\hat{\mathbf{x}}=\left(\mathbf{A}^{\mathrm{T}}\mathbf{A}\right)^{-1}\mathbf{A}^{\mathrm{T}}\mathbf{b}. \tag{37}$$

Since the second derivative of $\mathbf{P}(\mathbf{x})$ with respect to x $\frac{\partial^2\mathbf{P}(\hat{\mathbf{x}})}{\partial\hat{\mathbf{x}}^2}=2\mathbf{A}^{\mathrm{T}}\mathbf{A}$ is positive definite, $\mathbf{P}(\mathbf{x})$ is minimized when the derivative is 0. Then the estimation error $\delta\mathbf{x}$ is defined as

$$\begin{aligned}\delta\mathbf{x}&=\mathbf{x}-\left(\mathbf{A}^{\mathrm{T}}\mathbf{A}\right)^{-1}\mathbf{A}^{\mathrm{T}}\mathbf{b}\\ &=\mathbf{x}-\left(\mathbf{A}^{\mathrm{T}}\mathbf{A}\right)^{-1}\mathbf{A}^{\mathrm{T}}(\mathbf{A}\mathbf{x}+n)\\ &=-\left(\mathbf{A}^{\mathrm{T}}\mathbf{A}\right)^{-1}\mathbf{A}^{\mathrm{T}}\mathbf{n}.\end{aligned} \tag{38}$$

According to (38), the least squares estimation is only related to the system transformation relation vector A and the system noise N. When N follows a Gaussian distribution with a mean of 0, the estimation of LSM is unbiased. Since LSM can only solve linear equations, it is necessary to transform the problem into a linear one.

We then define that $\rho_{ci}(\mathbf{x}_{r0})$ denotes the corrected pseudo-range between satellite s_i and initial solution, which is expressed as

$$\begin{aligned}\rho_{ci}(\mathbf{x}_{r0})&=\sqrt{(x_i-x_{u0})^2+(y_i-y_{u0})^2+(z_i-z_{u0})^2}\\ &\quad+c\Delta t_{r0}\\ &=r_i(\mathbf{x}_{r0})+c\Delta t_{r0},\end{aligned} \tag{39}$$

where $r_i(\mathbf{x}_{r0})$ represents the Euclidean distance from satellite s_i to initial solution.

Then, the positioning equations is transformed into

$$\begin{aligned}&\begin{bmatrix}\rho_{c1}(\mathbf{x}_r)-\rho_{c1}(\mathbf{x}_{r0})\\ \rho_{c2}(\mathbf{x}_r)-\rho_{c2}(\mathbf{x}_{r0})\\ \rho_{c3}(\mathbf{x}_r)-\rho_{c3}(\mathbf{x}_{r0})\\ \rho_{c4}(\mathbf{x}_r)-\rho_{c4}(\mathbf{x}_{r0})\end{bmatrix}=\\ &\begin{bmatrix}\frac{x_1-x_{r0}}{r_1(\mathbf{x}_{r0})} & \frac{y_1-y_{r0}}{r_1(\mathbf{x}_{r0})} & \frac{z_1-z_{r0}}{r_1(\mathbf{x}_{r0})} & c\\ \frac{x_2-x_{r0}}{r_2(\mathbf{x}_{r0})} & \frac{y_2-y_{r0}}{r_2(\mathbf{x}_{r0})} & \frac{z_2-z_{r0}}{r_2(\mathbf{x}_{r0})} & c\\ \frac{x_3-x_{r0}}{r_3(\mathbf{x}_{r0})} & \frac{y_3-y_{r0}}{r_3(\mathbf{x}_{r0})} & \frac{z_3-z_{r0}}{r_3(\mathbf{x}_{r0})} & c\\ \frac{x_4-x_{r0}}{r_4(\mathbf{x}_{r0})} & \frac{y_4-y_{r0}}{r_4(\mathbf{x}_{r0})} & \frac{z_4-z_{r0}}{r_4(\mathbf{x}_{r0})} & c\end{bmatrix}\begin{bmatrix}x_u-x_{r0}\\ y_u-y_{r0}\\ z_u-z_{r0}\\ \Delta t_r-\Delta t_{r0}\end{bmatrix}\\ &+\begin{bmatrix}n_1\\ n_2\\ n_3\\ n_4\end{bmatrix}.\end{aligned} \tag{40}$$

Hence, we can calculate the positioning for satellite s_i by the following equation

$$\delta\rho_{ci}=\mathbf{u}_i(\mathbf{A}^T\mathbf{A})^{-1}\mathbf{A}^T\mathbf{b}+n_0. \tag{41}$$

The current solution $\mathbf{x}_{r1}$ can be then updated, which can be

expressed as

$$\mathbf{x}_{r1} = \mathbf{x}_{r0} + (\mathbf{A}^T\mathbf{A})^{-1}\mathbf{A}^T\mathbf{b}. \tag{42}$$

C. Positioning accuracy

We first define a positioning error and clock error vector, which can be calculated from the pseudo-range measurement error as

$$\begin{bmatrix} \varepsilon_x & \varepsilon_y & \varepsilon_z & \varepsilon_t \end{bmatrix}^T = \left(\mathbf{A}^T\mathbf{A}\right)^{-1}\mathbf{A}^T\varepsilon_\rho, \tag{43}$$

where ε_ρ denotes the measurement error, which is independent and follows Gaussian distributions with mean 0 and variance σ^2_{URE}. In order to provide comprehensive performance analysis, we first derived the covariance of pseudo-range measurement error as

$$\begin{aligned} &Cov\left(\begin{bmatrix} \varepsilon_x & \varepsilon_y & \varepsilon_z & \varepsilon_t \end{bmatrix}^T\right) \\ &= \left(\mathbf{A}^T\mathbf{A}\right)^{-1}\sigma^2_{URE} \\ &= \mathbf{F}\sigma^2_{URE}, \end{aligned} \tag{44}$$

where $Cov(\cdot)$ denotes the covariance function. $\mathbf{F} = (\mathbf{A}^T\mathbf{A})^{-1}$ is the weight coefficient matrix, which is a fourth-order symmetric matrix.

It is clear that the measurement error is amplified by the weight coefficient matrix $\mathbf{F}$ and becomes the positioning error. σ_x^2, σ_y^2, σ_z^2 and σ_t^2 are the variances of positioning error, which correspond to the diagonal elements h_{11}, h_{22}, h_{33} and h_{44}, respectively. In this article, the PDoP is utilized to reveal the performance of the proposed networks, which is formulated as follows:

$$\begin{aligned} \mathrm{PDoP} &= \sqrt{\sigma_x^2 + \sigma_y^2 + \sigma_z^2} \\ &= \sqrt{h_{11} + h_{22} + h_{33}}. \end{aligned} \tag{45}$$

Note that based on the definition of PDoP, when the satellites are evenly distributed, PDoP becomes smaller, resulting in higher position accuracy.

IV. Passive Beamforming Design at RIS

In this article, we consider that the number of visible satellites is lower than 4. The STAR-RIS array is deployed to provide navigation and communication services to the users located in the urban canyon or indoor scenarios. Therefore, the STAR-RIS needs to select a proper satellite based on the different priorities mentioned in the following subsections.

A. Navigation-Prioritized Algorithm

In the urban canyons, the STAR-RIS array reflects the invisible satellites to the ground users to provide additional links. In order to provide higher accurate navigation services, we propose a novel NPA based on the PDoP by designing the passive beamforming at STAR-RIS, where the navigation accuracy of multiple users is optimized. To do so, we first define the position error as follows:

$$\varepsilon_u = \sqrt{(x - x_u)^2 + (y - y_u)^2 + (z - z_u)^2}, \tag{46}$$

where x, y and z are calculated position of user u. x_u, y_u and z_u are real position of user u.

In order to improve the positioning accuracy, the objective function can be given by:

$$\min_{s_{\text{sel}}} \quad \varepsilon_u(x, y, z), \tag{47a}$$

$$\text{s.t.} \quad \hat{\mathbf{x}} < \epsilon, \tag{47b}$$

$$n < n^*, \tag{47c}$$

$$s_{\text{sel}} \in I_n, \tag{47d}$$

where n^* is the maximum number of iterations of the least squares algorithm. $\hat{\mathbf{x}}$ is the correction of the least squares estimate. ϵ is the pre-set iteration threshold. s_{sel} is the satellite selected through RIS in the satellite selection method. (47b) represents a convergence constraint, which ensures that the step size in the final iteration does not exceed a predefined threshold. (47c) outlines a constraint on the number of iterations, ensuring that the number of iterations in the LSM algorithm must not exceed the maximum allowed. (47d) defines the satellite selection constraint, which specifies that the selected satellite must be visible.

We define that $F(\bullet)$ is the distance from the satellite to the user. $\bar{\mathbf{l}}$ is the pseudo-range matrix. $\mathbf{C}_\ell$ is the covariance matrix of measurements. $\mathbf{x}^0$ and $\bar{\mathbf{x}}$ respectively are the initial value of the iteration and the user position guessed based on the pseudo-range. $\mathbf{x}^{ls}$ is the least squares estimate. Then, in order to select the satellite providing the best positioning accuracy, a penalty-based algorithm has been proposed to solve the problem in (47). The algorithm iteratively evaluates each NLoS satellite in combination with the available LoS satellites to compute the PDoP. Within each iteration, a LSM loop is performed to estimate the solution vector. The loop terminates once the solution converges below a predefined threshold. Finally, the NLoS satellite that yields the minimum PDoP is selected. Thus, the **Algorithm 1** is given as follows.

Algorithm 1 Penalty-based iterative algorithm to solve problem (47)

repeat
  In the selecting loop: obtain the PDoP of each NLoS satellite combined with the LoS satellites
  repeat
    In the LSM loop: Perform the least squares method
    Establish $F(\bar{\mathbf{x}}) = \bar{\mathbf{l}}$
    Initialize $\mathbf{x}^0 \cong \bar{\mathbf{x}}$ and $\mathbf{A}\mathbf{x} = \mathbf{b} + \mathbf{v}$
    initialize the iteration index $\mathrm{n} = 0$, solve $\mathbf{A}^{\mathrm{T}}\mathbf{A}\hat{\mathbf{x}} = \mathbf{A}^{\mathrm{T}}\mathbf{b}$
    $\hat{\mathbf{x}} = \left(\mathbf{A}^{\mathrm{T}}\mathbf{A}\right)^{-1}\mathbf{A}^{\mathrm{T}}\mathbf{b}$
    $\mathbf{x}^{ls} = \mathbf{x}^0 + \hat{\mathbf{x}}$
  until $\hat{\mathbf{x}}$ is below ϵ.
until all the NLoS satellites have been traversed.
Select the NLoS satellite which minimizes the PDoP.

With the aid of **Algorithm 1**, the satellite providing the best positioning performance can be selected by the NPA. Then, we can have following remarks.

Remark 1: The results in **Algorithm 1** demonstrate that although STAR-RIS can provide additional LoS links from satellite to users, a STAR-RIS array can only provide users with one virtual LoS link, that is, each STAR-RIS array can

only introduce a maximum of one non-directly connected satellite. Therefore, the STAR-RIS to indoor user link is shared by multiple satellites, resulting in high positioning errors.

Remark 2: The results in **Algorithm 1** demonstrate that in order to improve the PDoP performance, the satellite with higher geometric diversity is expected for the NPA.

Remark 3: In the proposed indoor scenario, the shared distance between the STAR-RIS and the indoor user will be considered as non-identical-and-independent interference in (40), which cannot be mitigated by using the LSM algorithm.

Based on **Algorithm 1**, the NPA exhibits dual applications. Primarily, it facilitates simultaneous communication and navigation functionalities for users encountering a scarcity of directly accessible satellites. Secondly, it serves to supplement satellite provision, thereby enhancing positional accuracy for users experiencing low precision in positioning.

Complexity Analysis: Unlike NPA, since the CPA only selects the satellite with the nearest distance, its computational complexity mainly depends on the number of STAR-RIS elements and users, while the number of satellites has a negligible impact on complexity.

B. Communication-Prioritized Algorithm

On the contrary, we also focuses on the communication performance of both the indoor and outdoor users. It is assumed that the INAC satellite is the i-th satellite. Therefore, we then propose a CPA for maximizing the achievable ergodic rate of users, where the objective function of CPA can be given by:

$$\begin{aligned} &\max_{\theta_{1,R},\theta_{1,T}} \; R_R + R_T \\ &\text{subject to } \beta_{1,R}\cdots\beta_{N,R} = 0.5 \\ &\qquad\quad \beta_{1,T}\cdots\beta_{N,T} = 0.5 \\ &\qquad\quad \theta_{1,R}\cdots\theta_{N,R} \in [0, 2\pi) \\ &\qquad\quad \theta_{1,T}\cdots\theta_{N,T} \in [0, 2\pi)\,, \end{aligned} \tag{48}$$

where R_R and R_T respectively represent the achievable ergodic rate of the reflected and indoor users.

Given that navigation data requirements are substantially lower than that of communications, the passive beamforming at the STAR-RIS is designed primarily to optimize channel gains for both indoor and outdoor users. Consequently, the objective functions can be re-formulated as follows:

$$\begin{aligned} &\max_{\theta_{1,R}} \left|\mathbf{g}_u \mathbf{\Psi}_R \mathbf{h}_R \sqrt{L_{Riu}} + h_{iu}\sqrt{L_{iu}}\right|^2 \\ &\max_{\theta_{1,T}} \left|\mathbf{g}_u \mathbf{\Psi}_T \mathbf{h}_R \sqrt{L_{Riu}}\right|^2 \\ &\text{subject to } \beta_{1,R}\cdots\beta_{N,R} = 0.5 \\ &\qquad\quad \beta_{1,T}\cdots\beta_{N,T} = 0.5 \\ &\qquad\quad \theta_{1,R}\cdots\theta_{N,R} \in [0, 2\pi) \\ &\qquad\quad \theta_{1,T}\cdots\theta_{N,T} \in [0, 2\pi)\,. \end{aligned} \tag{49}$$

Therefore, by employing the signal alignment technique, as detailed in [24], our goal can be realized to effectively enhance the received power. To configure the phase shifts appropriately, the reflection channel vector and the transmission channel vector are defined as follows:

$$\tilde{\mathbf{h}}_R = \left[\; g_{R,1u}h_{R,i1} \quad \cdots \quad g_{R,Nu}h_{R,iN} \;\right], \tag{50}$$

and

$$\tilde{\mathbf{h}}_T = \left[\; g_{T,1u}h_{R,i1} \quad \cdots \quad g_{T,Nu}h_{R,iN} \;\right]. \tag{51}$$

Thus, the reflection and transmission phase shifts arrays of the STAR-RISs can be further transformed into

$$diag(\arg(\mathbf{\Psi}_R)) = \theta_{\mathrm{d}} - \arg(\tilde{\mathbf{h}}_R), \tag{52}$$

and

$$diag(\arg(\mathbf{\Psi}_T)) = \theta_{\mathrm{d}} - \arg(\tilde{\mathbf{h}}_T), \tag{53}$$

where $\arg(\cdot)$ denotes the angle of the element, and θ_{d} represents the desired phase, which can be set to any value. By implementing this approach, optimal channel gain is ensured for both indoor and outdoor users, allowing the objective function specified in (49) to be successfully achieved.

Then, the achievable ergodic rate of the outdoor and indoor users serving by the i-th INAC satellite can be given by:

$$R_{\mathrm{R},i} = \log_2\left(1 + \frac{\left(\sum_{n=1}^{N}\left|\beta_{1,R}g_{R,1u}h_{R,i1}\sqrt{L_{Riu}}\right| + \left|h_{iu}\sqrt{L_{iu}}\right|\right)^2}{\sigma^2}\right), \tag{54}$$

and

$$R_{\mathrm{T},i} = \log_2\left(1 + \frac{\left(\sum_{n=1}^{N}\left|\beta_{1,T}g_{T,1u}h_{R,i1}\sqrt{L_{Tiu}}\right|\right)^2}{\sigma^2}\right). \tag{55}$$

We then can compare the communication performance of different satellites, where the satellite providing the maximum achievable ergodic rate can be selected for the CPA as shown in **Algorithm 2** to solve problem (47). The algorithm begins by establishing the necessary parameters for all available INAC satellites, including channel vectors, reflection and transmission coefficients, and path-loss related parameters. It then initializes the STAR-RIS phase shift matrices for reflection and transmission. During each iteration, the algorithm computes the optimized passive beamforming matrices to evaluate the achievable ergodic rate for the user associated with each available satellite. After traversing all potential satellites, the algorithm selects the proper INAC satellite that maximizes the user's ergodic rate, thereby enabling an efficient joint optimization of communication performance and satellite selection.

Remark 4: The results in **Algorithm 2** indicate that by utilizing SIC technique, the CO-INAC scenario is capable of providing higher achievable ergodic rate in the high SNR regimes.

Remark 5: The results in **Algorithm 2** demonstrate that in order to improve the achievable ergodic rate performance, the nearest satellite is expected for the CPA.

Algorithm 2 CPA to solve problem (49)

1: Establish $\mathbf{g}_u$, $\mathbf{\Psi}_R$, $\mathbf{h}_R$, $\mathbf{h}_{iu}$, $\sqrt{L_{Riu}}$ and $\sqrt{L_{iu}}$ for all available INAC satellites
2: Initialize $\mathbf{\Psi}_R$ and $\mathbf{\Psi}_T$
3: **repeat**
4: Obtain the reflection and transmission passive beamforming matrix of STAR-RIS
5: Calculate the achievable ergodic rate of user by each INAC satellite.
6: **until** All the satellites have been traversed.
7: Select the INAC satellite which maximizes the achievable ergodic rate.

Complexity Analysis: Since the NPA primarily focuses on satellite selection, its computational complexity mainly depends on the number of satellites and users, while the number of STAR-RIS elements has a negligible impact on complexity.

V. Numerical Results

In this section, numerical results are provided for the performance evaluation of the proposed NPA and CPA assisted INAC networks. As shown in Fig. 1, the STAR-RIS is located at the window of the building to provide access services to indoor and outdoor users. The iteration number of the least squares method is set to 2000 times, where the accuracy is set to 0.1 meters. We then select 10 available satellites, where the locations are shown in Table I.

Without loss of generality, we assume that the propagation environment for outdoor users follows urban canyon scenarios, where the details of surrounding buildings are ignored for simplicity. The main parameters are set according to typical settings in satellite-terrestrial networks [50]. Note that the ionospheric and tropospheric delays are considered constant. Therefore, we simply omitted the ionospheric and tropospheric delays from the simulations. Consequently, the navigation performance is impacted solely by the multipath effect and receiver noise correlations. The path loss exponents of $s_i - STAR-RIS$, $s_i - user_u$, as well as $STAR-RIS-user_u$ links are set to 2, 2, as well as 2.2, respectively. The transmit power at each satellite is set to 40 W. The transmit antenna gain is set to 30 dB. The carrier frequency is set to 1 GHz. The bandwidth is set to $BW = 10$ MHz. The power of AWGN is set to $-174 + 10\log(BW)$. The reflection and transmission phases of STAR-RIS are continuous, and the amplitude coefficient of each RIS element is identity. For simplicity, we set the reflection amplitude coefficient and transmission amplitude coefficient to 0.5. Based on the insight of [49], the small-scale fading parameters of the shadow Rician fading channels are set to $b = 0.279$, $m = 2$, as well as $\Omega = 0.251$. In order to better illustrate the performance, we do not consider the effect of atmospheric time delay and other influencing factors.

A. Impact of Satellite Selection for Positioning Accuracy

In this subsection, we evaluate the positioning error of both the indoor and outdoor users by NPA in Fig. 3 for 500 independent realizations of the instantaneous noise. The number of visible satellites of outdoor users and indoor users is set to 3 and 0, respectively. On the one hand, in Fig. 3, the STAR-RIS connects one satellite to the outdoor user for providing positioning services. On the other hand, since there is no direct link between satellites and indoor users, the STAR-RIS connects four satellites to the indoor user. Observe that when the PDoP increases, the positioning error of both indoor and outdoor users increases. This is due to the fact that high PDoP indicates poorer geometry distribution of satellites, resulting in higher positioning errors. As can be seen from the red and purple curves in Fig. 3, the positioning error of indoor users is much higher than that of the outdoor user, which is because that the STAR-RIS to indoor user link is shared by all satellites. For example, when the distance between STAR-RIS and the indoor user is 10 meters, and compared to the positioning error of outdoor users, the positioning error of the indoor user also increases by 10 meters. This phenomenon also verifies our **Remark 1**. In addition, it is also confirmed that the positioning error is mainly related to the distance between STAR-RIS and the indoor user, which validate our **Remark 3**.

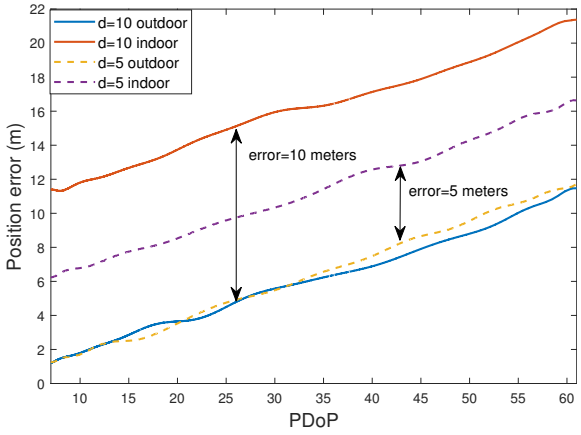

Fig. 3. The positioning error versus PDoP of both outdoor and indoor users.

Here, we evaluate the positioning error of both the indoor and outdoor users with the aid of NPA with different number of satellites for 500 independent realizations in Fig. 4. For comparison, we denote the random satellite selection algorithm as "RSA" in Fig. 4, for which we assume that the STAR-RIS connects a random satellite. In Fig. 4, there are a total of 11 available satellites in the proposed INAC networks. For the outdoor users, there are at least 3 visible satellites, whereas there is no visible satellite for the indoor users. As we can observe from Fig. 4, the proposed NPA has superior performance than that of the RSA for both indoor and outdoor users. We also observe that increasing the number of connected satellites can improve positioning performance when the total number of satellites is relatively low. However, once the number of satellites is sufficiently high, connecting an additional satellite via STAR-RIS does not provide further performance gains, as it does not improve the PDoP. It is also noted that the minimum positioning error of the indoor user is higher than 5 meters, which indicates that for the indoor users,

TABLE I:
TABLE OF LOCATIONS

Target	X-axis coordinates	Y-axis coordinates	Z-axis coordinates
STAR-RIS	2451473.43334794	2940007.18127632	5084877.94326077
Indoor user	2451523.43334794	2940057.18127632	5084857.94326077
Outdoor user	2451423.43334794	2939957.18127632	5084827.94326077
Satellite 1	2384140.77986545	26292387.6749704	-1752765.80294385
Satellite 2	-7688937.22670325	13088957.6457098	21791665.4813813
Satellite 3	7694983.70804847	-12857727.5493792	22058611.9934355
Satellite 4	21593131.9113028	14858836.7899355	-4809198.45852993
Satellite 5	14735759.3485476	3642752.94843750	21710269.2023414
Satellite 6	10822949.9268744	17448224.4300194	16861015.1148962
Satellite 7	22983405.0752494	-2550895.23789826	13042468.3643485
Satellite 8	15960648.1354986	-4443134.15738840	20811348.4358723
Satellite 9	23113652.8643512	1123278.14965420	6871538.15438270
Satellite 10	16937593.1345824	-14466934.1345798	-14539112.5683248

no matter how many satellites are connected to the indoor users through STAR-RIS, the positioning error mainly depends on the distance between STAR-RIS and indoor users, which also verifies both **Remark 1** and **Remark 2**. Observe that when the number of satellites exceeds 9, the positioning error increases due to the impact of noise, indicating the existence of an optimal number of connected satellites.

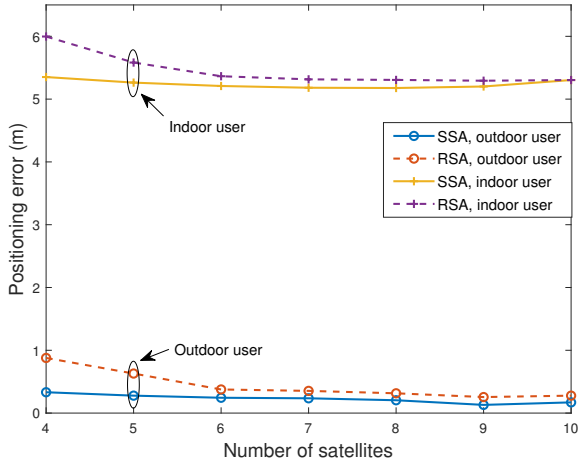

Fig. 4. The positioning error versus the number of satellites, where the distance between STAR-RIS and both indoor and outdoor user is set to 5 meters.

We evaluate the positioning error of both the indoor and outdoor users with the increasing distance between STAR-RIS and user in Fig. 5 for 100 independent realizations of the instantaneous noise. Fig. 5 clearly shows that the positioning error is significantly lower for outdoor users compared to indoor users, which is expected due to the better propagation conditions in outdoor environments. In addition, the positioning error for the outdoor user remains very small and stable across all distances between the STAR-RIS and the user, suggesting that the outdoor environment yields more accurate positioning. On the contrary, for the indoor user, the positioning error increases steadily as the distance between the STAR-RIS and the user increases. This indicates that greater distances in indoor environments lead to more significant positioning errors, which confirm our **Remark 3**.

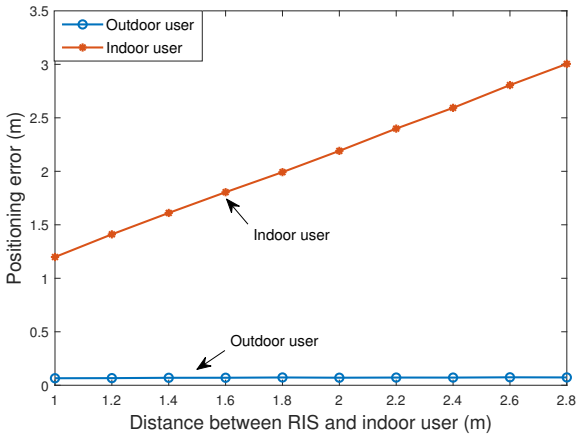

Fig. 5. The positioning error for both indoor and outdoor users versus the distance between STAR-RIS and user.

B. The Impact of Satellite Selection for Transmit Power

In Fig. 6, we focus our attention on the minimum transmit power with different numbers of STAR-RIS elements in both the NO-INAC and CO-INAC scenarios. The minimum rates of the indoor and outdoor users are set to 1 and 2 bits, respectively. The minimum required SNR threshold is set to 0.7, which is 5.3 dB. The power allocation factors are respectively set to $\omega_C = 0.65$ and $\omega_N = 0.35$. As can be seen from Fig. 6, when more STAR-RIS elements are deployed, the required transmit power decreases. This is obviously due to the fact that the signal transmitted or reflected by STAR-RIS can be perfectly boosted at users, resulting in a lower transmit power requirement. On the other hand, we can also observe that in both CO-INAC and NO-INAC scenarios, the transmit power requirement of navigation signals is higher than that of the communication signals, which indicates that more power is expected for the navigation signal.

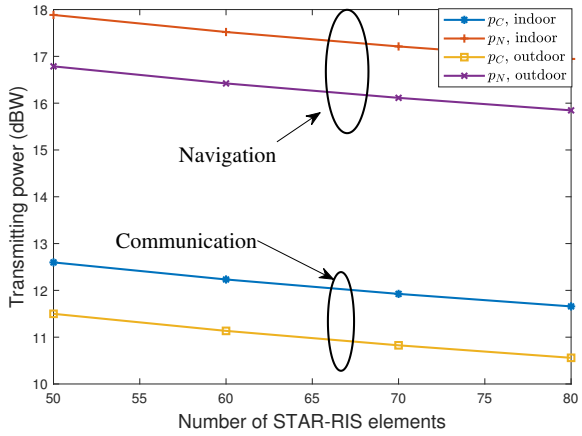

Fig. 6. The minimum transmit power versus the number of STAR-RIS elements.

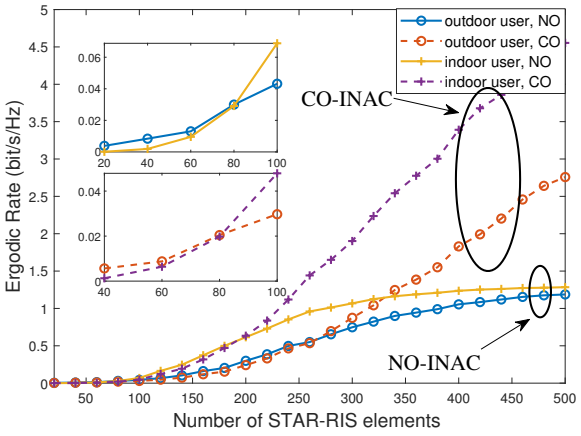

Fig. 8. The achievable ergodic rate of the indoor and outdoor users in both the CO-INAC and NO-INAC scenarios.

C. The Impact of directly connected satellites on PDoP

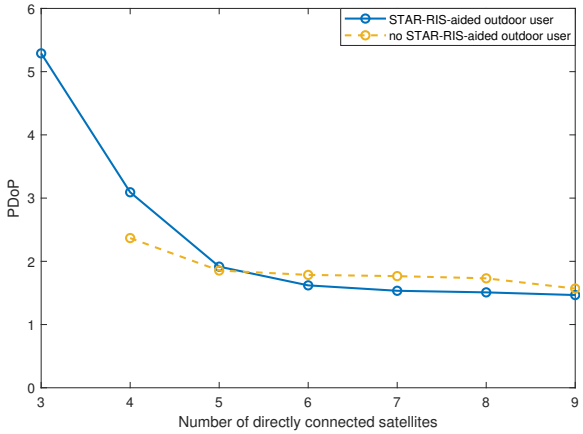

Fig. 7. The PDoP versus the number of directly connected satellites.

Let us continue to analyze the number of directly connected satellites on PDoP in Fig. 7. In order to better illustrate the performance of the proposed networks, the PDoP of the outdoor user without STAR-RIS is also considered, denoted as "no-RIS". Note that when there is no STAR-RIS, and the number of directly connected satellites is 3, the PDoP does not exist. On the contrary, with the aid of STAR-RIS, only 3 directly connected satellites are capable of providing navigation services, which illustrates the superiority of the proposed satellite selection networks. By comparing two curves in Fig. 7, we can also observe that the PDoP floor of the STAR-RIS-aided networks is lower than that of "no-RIS" scenario, which is because that the location of STAR-RIS also improves the PDoP performance.

D. The Achievable Ergodic Rate

In Fig. 8, we focus our attention on the achievable ergodic rate in the NO-INAC and CO-INAC scenarios. The power allocation factors are respectively set to $\omega_C = 0.8$, $\omega_N = 0.2$ and $\omega_C = 0.2$, $\omega_N = 0.8$ for the NO-INAC and CO-INAC scenarios. The achievable ergodic rates of the indoor and outdoor users are averaged by 1000 independent Monte Carlo simulations. Note that we only focus on the achievable ergodic rate of communications, where the navigation rate is ignored in Fig. 8. Observe that in the NO-INAC scenarios, the achievable ergodic rate ceilings of both the indoor and outdoor users occur, which indicates that the NO-INAC scenario is only suitable for the case with low data rate requirements. On the contrary, we can see that the achievable ergodic rate of both the indoor and outdoor users increases with the aid of STAR-RIS arrays. In addition, the achievable ergodic rate of the indoor user is higher than that of the outdoor user when the number of STAR-RIS elements is high enough. This is because that the STAR-RIS is closer to the indoor user, leading to the higher SNR in the high STAR-RIS element case. The simulation results in Fig. 8 verify our **Remark 4**, where CO-INAC scenario is expected for higher achievable ergodic rate performance.

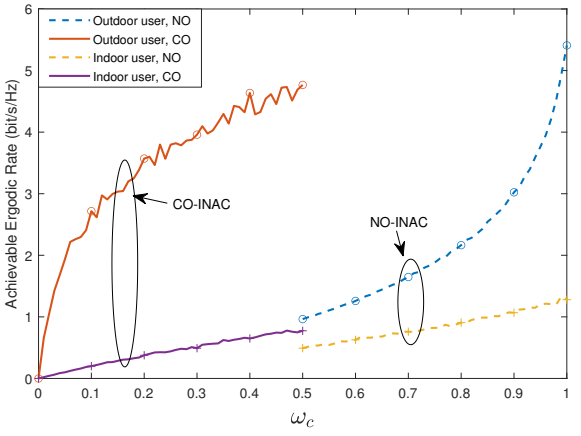

Fig. 9. The achievable ergodic rate versus the power allocation factors.

We then turn our attention to the impact of power allocation factors. It is noted that in the CO-INAC scenarios, the power allocation factor of communication is lower than 0.5, whereas the power allocation factor of communication is higher than

0.5 in the NO-INAC scenarios. The transmit power is set to 46 dBm, and the number of STAR-RIS elements is set to 50. As we can see from Fig. 9, it is observed that the achievable ergodic rate increases with the increasing power allocation factor in both CO-INAC and NO-INAC scenarios. This is due to the fact that when the number of RIS elements is sufficiently high, the received SINR is mainly dominated by the power allocation factors. This phenomenon also indicates that a hybrid CO/NO-INAC selection algorithm is preferable. Moreover, since the power allocation factor cannot be higher than 1, the achievable ergodic rate performance of the CO-INAC scenarios outperforms than that of the NO-INAC scenarios, which confirms our **Remark 4**.

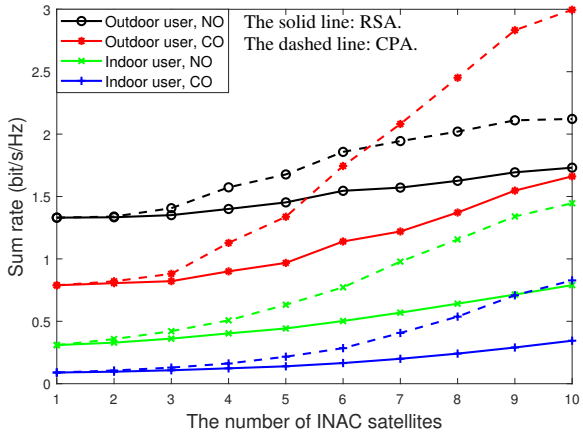

Fig. 10. The sum rate versus the number of satellites, where CPA and RSA are compared.

Here, we evaluate the sum rate of both the indoor and outdoor users with the aid of CPA with different number of satellites for 1000 independent realizations in Fig. 10. The parameters are identical as Fig. 4, for which we assume that the STAR-RIS connects a satellite with best communication performance. As can be observed that the CPA outperforms RSA across all user types, which verifies the effectiveness of our proposed CPA. This also verifies our **Remark 5**. We can also observe that the sum rate gap for indoor users is more pronounced, which is because that the distance between STAR-RIS and the indoor user is much smaller than that of the outdoor user.

In Fig 11, We then compare the impact of distance between the INAC satellite and STAR-RIS to the positioning error and achievable ergodic rate in the CO-INAC scenarios. Note that only one INAC satellite and three navigation satellites are available, where the height of the orbit are identical. Therefore, when the distance between the INAC satellite and STAR-RIS increases, where the elevation angle between the INAC satellite and ground user decreases, the PDoP can be decreased, resulting in a lower positioning error. On the contrary, we can observe that when the distance between the INAC satellite and RIS increases, the achievable ergodic rate decreases due to the increasing large-scale fading. In addition, with the increasing distance, the positioning error has its performance floor, whereas the achievable ergodic rate decreases with the increasing distance. This phenomenon also indicates the trade-

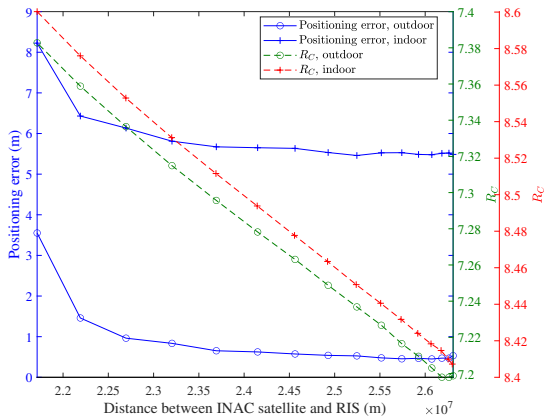

Fig. 11. The comparison between positioning error and achievable ergodic rate versus the distance between INAC satellite and STAR-RIS.

off between positioning error and the achievable ergodic rate of the proposed satellite selection algorithm, which confirms both **Remark 2** and **Remark 5**.

VI. Conclusion

In this article, we introduced a STAR-RIS-assisted INAC network to address the challenges of urban canyon positioning. Initially, we outlined the existing difficulties faced by current positioning technologies and discussed the benefits of utilizing STAR-RIS. Building on traditional models, we developed a STAR-RIS-assisted INAC network, strategically designing the NPA and CPA of the STAR-RIS array. We evaluated the network's performance by analyzing the positioning error and achievable ergodic rate, demonstrating its effectiveness in both navigation and communication. This investigation lays the groundwork for future advancements in STAR-RIS technology to meet the increasing demands for accurate and reliable GNSS services in obstructed environments. The findings indicate that the positioning error of the indoor user mainly depends on the distance between STAR-RIS and indoor users. Some potential future directions are summarized as follows:

- One potential future direction is to minimize the positioning error of indoor users by incorporating additional available information, such as time synchronization. Furthermore, deploying additional STAR-RIS arrays can provide additional data for navigation.
- Increasing the number of STAR-RIS elements is capable of enhancing the estimation accuracy of azimuth and elevation angles. Therefore, the impact of RIS on positioning accuracy warrants further investigation.
- Alternatively, if the RIS array aperture is sufficiently large, techniques like near-field sensing could be employed when other information is unavailable.

References

[1] N. Can, "Liability for GNSS signals and services," in *2017 8th International Conference on Recent Advances in Space Technologies (RAST)*, Jun. 2017, pp. 529–533.

[2] J. Bruzual, E. Lacarra, C. Post, and J. R. González, "Infield Agriculture GNSS Assessment Showing EGNOS Benefits," in *2020 European Navigation Conference (ENC)*, 2020, pp. 1–10.

[3] D. Lu, D. Spiegel, U. Becker, B. Cai, J. Wang, J. Liu, and X. Liu, "Repeatability test method of GNSS for safe train localisation in real and simulated environments," in *2016 IEEE/ION Position, Location and Navigation Symposium (PLANS)*, 2016, pp. 687–692.

[4] C. Counselman *et al.*, "Backpack VLBI terminal with subcentimeter capability," *NASA. Goddard Space Flight Center Radio Interferometry*, no. 3, pp. 409–414, Jun. 1980.

[5] S. Elmeadawy and R. M. Shubair, "6G Wireless Communications: Future Technologies and Research Challenges," in *2019 International Conference on Electrical and Computing Technologies and Applications (ICECTA)*, 2019, pp. 1–5.

[6] G. Seco-Granados, J. López-Salcedo, D. Jiménez-Baños, and G. López-Risueño, "Challenges in Indoor Global Navigation Satellite Systems: Unveiling its core features in signal processing," *IEEE Signal Process. Mag*, vol. 29, no. 2, pp. 108–131, Mar. 2012.

[7] A. L. A. Steingass, "Land Mobile Satellite Navigation-Characteristics of the Multipath Channel," in *Proceedings of the 16th International Technical Meeting of the Satellite Division of The Institute of Navigation(ION GPS/GNSS 2003)*, Portland, OR, Sep. 2003, pp. 1016–1022.

[8] E. Elezi, G. Çankaya, A. Boyacı, and S. Yarkan, "A detection and identification method based on signal power for different types of Electronic Jamming attacks on GPS signals," in *2019 IEEE 30th Annual International Symposium on Personal, Indoor and Mobile Radio Communications (PIMRC)*, 2019, pp. 1–5.

[9] G. Gao and G. Lachapelle, "INS-assisted high sensitivity GPS receivers for degraded signal navigation," *Proceedings of the 19th International Technical Meeting of the Satellite Division of the Institute of Navigation*, pp. 2977–2989, 2006.

[10] R. S. Kulikov and A. I. Perov, "Navigation of vehicle in urban canyon via two-satellite GNSS and map aiding," in *2017 Dynamics of Systems, Mechanisms and Machines (Dynamics)*, 2017, pp. 1–7.

[11] A. Broumandan, J. Nielsen, and G. Lachapelle, "Enhanced detection performance of indoor GNSS signals based on synthetic aperture," *IEEE Trans. Veh. Tech.*, vol. 59, no. 6, pp. 2711–2724, Jul. 2010.

[12] H. Hadidianmoghadam and A. B. Kouki, "New modified urban canyon models for satellite signal propagation prediction," *IEEE Access*, vol. 7, pp. 25 298–25 307, 2019.

[13] H. More, E. Cianca, and M. De Sanctis, "Positioning performance of LEO mega constellations in deep urban canyon environments," in *2022 25th International Symposium on Wireless Personal Multimedia Communications (WPMC)*, 2022, pp. 256–260.

[14] Z. Xu, G. Chen, R. Fernandez, Y. Gao, and R. Tafazolli, "Enhancement of Direct LEO Satellite-to-Smartphone Communications by Distributed Beamforming," *IEEE Trans. Veh. Technol.*, vol. 73, no. 8, pp. 11 543–11 555, Aug. 2024.

[15] M. A. ElMossallamy, H. Zhang, L. Song, K. G. Seddik, Z. Han, and G. Y. Li, "Reconfigurable Intelligent Surfaces for Wireless Communications: Principles, Challenges, and Opportunities," *IEEE Trans. Cognit. Commun. Networking*, vol. 6, no. 3, pp. 990–1002, Sep. 2020.

[16] C. Liaskos, S. Nie, A. Tsioliaridou, A. Pitsillides, S. Ioannidis, and I. Akyildiz, "A New Wireless Communication Paradigm through Software-Controlled Metasurfaces," *IEEE Commun. Mag.*, vol. 56, no. 9, pp. 162–169, Sep. 2018.

[17] H. Qiu, S. Gong, H. Liu, X. Zhao, and C. Xing, "Active-Passive Beamforming Optimization for RIS-Aided mmWave Joint Localization and Communication System," *IEEE Trans. Veh. Tech.*, vol. 74, no. 2, pp. 2941–2957, Feb. 2025.

[18] H. Li, R. Liu, M. Liy, Q. Liu, and X. Li, "IRS-Enhanced Wideband MU-MISO-OFDM Communication Systems," in *2020 IEEE Wireless Communications and Networking Conference (WCNC)*, 2020, pp. 1–6.

[19] H. Li, W. Cai, Y. Liu, M. Li, Q. Liu, and Q. Wu, "Intelligent Reflecting Surface Enhanced Wideband MIMO-OFDM Communications: From Practical Model to Reflection Optimization," *IEEE Trans. Commun.*, vol. 69, no. 7, pp. 4807–4820, Jul. 2021.

[20] Z. Li, M. Hua, Q. Wang, and Q. Song, "Weighted Sum-Rate Maximization for Multi-IRS Aided Cooperative Transmission," *IEEE Wireless Commun. Lett.*, vol. 9, no. 10, pp. 1620–1624, Oct. 2020.

[21] Y. Yang, B. Zheng, S. Zhang, and R. Zhang, "Intelligent Reflecting Surface Meets OFDM: Protocol Design and Rate Maximization," *IEEE Trans. Commun.*, vol. 68, no. 7, pp. 4522–4535, Jul. 2020.

[22] C. Huang, A. Zappone, M. Debbah, and C. Yuen, "Achievable Rate Maximization by Passive Intelligent Mirrors," in *2018 IEEE International Conference on Acoustics, Speech and Signal Processing (ICASSP)*, 2018, pp. 3714–3718.

[23] Y. Liu, X. Liu, X. Mu, T. Hou, J. Xu, M. Di Renzo, and N. Al-Dhahir, "Reconfigurable Intelligent Surfaces: Principles and Opportunities," *IEEE Commun. Surv. Tutor.*, vol. 23, no. 3, pp. 1546–1577, thirdquarter 2021.

[24] T. Hou, Y. Liu, Z. Song, X. Sun, Y. Chen, and L. Hanzo, "Reconfigurable Intelligent Surface Aided NOMA Networks," *IEEE J. Sel. Areas Commun.*, vol. 38, no. 11, pp. 2575–2588, Nov. 2020.

[25] S. Zheng, B. Lv, T. Zhang, Y. Xu, G. Chen, R. Wang, and P. C. Ching, "On DoF of Active RIS-Assisted MIMO Interference Channel With Arbitrary Antenna Configurations: When Will RIS Help?" *IEEE Trans. Veh. Technol.*, vol. 72, no. 12, pp. 16 828–16 833, Dec. 2023.

[26] J. Li, G. Chen, T. Zhang, W. Feng, W. Jiang, T. Q. S. Quek, and R. Tafazolli, "UAV-RIS-aided space-air-ground integrated network: Interference alignment design and dof analysis," *IEEE Trans. Wireless Commun.*, vol. 23, no. 9, pp. 11 678–11 692, Sep. 2024.

[27] I. Chatzigeorgiou, "The Impact of 5G Channel Models on the Performance of Intelligent Reflecting Surfaces and Decode-and-Forward Relaying," in *2020 IEEE 31st Annual International Symposium on Personal, Indoor and Mobile Radio Communications*, 2020, pp. 1–4.

[28] B. Di, H. Zhang, L. Song, Y. Li, Z. Han, and H. V. Poor, "Hybrid Beamforming for Reconfigurable Intelligent Surface based Multi-User Communications: Achievable Rates With Limited Discrete Phase Shifts," *IEEE J. Sel. Areas Commun.*, vol. 38, no. 8, pp. 1809–1822, Aug. 2020.

[29] M. Abuyaghi, S. Si-Mohammed, G. Shaker, and C. Rosenberg, "Positioning in 5G Networks: Emerging Techniques, Use Cases, and Challenges," *IEEE Internet Things J.*, vol. 12, no. 2, pp. 1408–1427, Jan. 2025.

[30] Q. Zhao, W. Gong, T. Hou, X. Sun, and E. Bodanese, "Global navigation satellite system (GNSS): A reconfigurable intelligent surface (RIS)-aided approach," in *GLOBECOM 2022 - 2022 IEEE Global Communications Conference*, 2022, pp. 3162–3167.

[31] M. Eskandari and A. V. Savkin, "Deep reinforcement learning based joint 3D navigation and phase shift control for mobile internet of vehicles assisted by RIS-equipped UAVs," *IEEE Internet of Things J.*, vol. 10, no. 20, pp. 18 054–18 066, Oct. 2023.

[32] M. Eskandari, A. V. Savkin, and W. Ni, "Consensus-based autonomous navigation of a team of RIS-equipped UAVs for LoS wireless communication with mobile nodes in high-density areas," *IEEE Trans. Autom. Sci. Eng.*, vol. 20, no. 2, pp. 923–935, Apr. 2023.

[33] Y. Liu, X. Mu, J. Xu, R. Schober, Y. Hao, H. V. Poor, and L. Hanzo, "STAR: simultaneous transmission and reflection for 360° coverage by intelligent surfaces," *IEEE Wireless Commun.*, vol. 28, no. 6, pp. 102–109, Dec. 2021.

[34] J. Xu, Y. Liu, X. Mu, and O. A. Dobre, "STAR-RISs: Simultaneous transmitting and reflecting reconfigurable intelligent surfaces," *IEEE Commun. Lett.*, vol. 25, no. 9, pp. 3134–3138, Sep. 2021.

[35] X. Mu, Y. Liu, L. Guo, J. Lin, and R. Schober, "Simultaneously transmitting and reflecting (STAR) RIS aided wireless communications," *IEEE Trans. Wireless Commun.*, vol. 21, no. 5, pp. 3083–3098, May 2022.

[36] J. Xu, X. Mu, J. T. Zhou, and Y. Liu, "Simultaneously transmitting and reflecting (STAR)-RISs: Are they applicable to dual-sided incidence?" *IEEE Wireless Commun. Lett.*, vol. 12, no. 1, pp. 129–133, Nov. 2023.

[37] Z. Wang, Z. Liu, Y. Shen, A. Conti, and M. Z. Win, "Location Awareness in Beyond 5G Networks via Reconfigurable Intelligent Surfaces," *IEEE J. Sel. Areas Commun.*, vol. 40, no. 7, pp. 2011–2025, Jul. 2022.

[38] H. Chen, P. Zheng, M. F. Keskin, T. Al-Naffouri, and H. Wymeersch, "Multi-RIS-Enabled 3D Sidelink Positioning," *IEEE Trans. Wireless Commun.*, vol. 23, no. 8, pp. 8700–8716, Aug. 2024.

[39] D. Avagnina, F. Dovis, A. Ghiglione, and P. Mulassano, "Wireless networks based on high-altitude platforms for the provision of integrated navigation/communication services," *IEEE Commun. Mag.*, vol. 40, no. 2, pp. 119–125, Feb. 2002.

[40] W.-Q. Wang and D. Jiang, "Integrated Wireless Sensor Systems via Near-Space and Satellite Platforms: A Review," *IEEE Sens. J.*, vol. 14, no. 11, pp. 3903–3914, Nov. 2014.

[41] L. Yin, Q. Ni, and Z. Deng, "A GNSS/5G Integrated Positioning Methodology in D2D Communication Networks," *IEEE J. Sel. Areas Commun.*, vol. 36, no. 2, pp. 351–362, Feb. 2018.

[42] K. Lee, H. Baek, and J. Lim, "Relay-based positioning in TDMA networks," *IEEE Systems Journal*, vol. 12, no. 4, pp. 3849–3852, Dec. 2018.

[43] J. Zeng, T. Lv, R. P. Liu, X. Su, M. Peng, C. Wang, and J. Mei, "Investigation on Evolving Single-Carrier NOMA Into Multi-Carrier NOMA in 5G," *IEEE Access*, vol. 6, pp. 48 268–48 288, 2018.

[44] Z. Ding, Y. Liu, J. Choi, Q. Sun, M. Elkashlan, I. Chih-Lin, and H. V. Poor, "Application of Non-Orthogonal Multiple Access in LTE and 5G Networks," *IEEE Commun. Mag.*, vol. 55, no. 2, pp. 185–191, Feb. 2017.
[45] Z. Ding, P. Fan, and H. V. Poor, "Impact of User Pairing on 5G Nonorthogonal Multiple-Access Downlink Transmissions," *IEEE Trans. Veh. Tech.*, vol. 65, no. 8, pp. 6010–6023, Aug. 2016.
[46] M. Cenk Ertürk, N. Hosseini, H. Jamal, A. Şahin, D. Matolak, and J. Haque, "Requirements And Technologies Towards Uam: Communication, Navigation, And Surveillance," in *2020 Integrated Communications Navigation and Surveillance Conference (ICNS)*, 2020, pp. 2C2–1–2C2–15.
[47] T. Hou and A. Li, "Performance analysis of NOMA-RIS aided integrated navigation and communication (INAC) networks," *IEEE Trans. Veh. Tech.*, vol. 72, no. 10, pp. 13 255–13 268, Oct. 2023.
[48] P. Zheng, X. Liu, and T. Y. Al-Naffouri, "LEO- and RIS-empowered user tracking: A riemannian manifold approach," *IEEE J. Sel. Areas Commun.*, vol. 42, no. 12, pp. 3445–3461, Dec. 2024.
[49] K. Li, J. Wang, T. Hou, A. Li, X. Yue, Y. Liu, and W. Chen, "Performance analysis of OMA/NOMA-aided satellite communication networks: A stochastic geometry approach," *IEEE Trans. Commun.*, vol. 73, no. 8, pp. 6577–6592, Aug. 2025.
[50] J. Du, D. Chizhik, R. A. Valenzuela, R. Feick, G. Castro, M. Rodriguez, T. Chen, M. Kohli, and G. Zussman, "Directional Measurements in Urban Street Canyons From Macro Rooftop Sites at 28 GHz for 90% Outdoor Coverage," *IEEE Trans. Antennas Propag.*, vol. 69, no. 6, pp. 3459–3469, Jun. 2021.

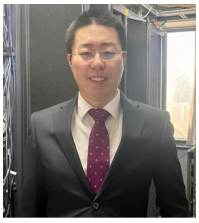

Tianwei Hou (S'19–M'21) received Ph.D. degree from Beijing Jiaotong University (BJTU) in 2021. He was a Post-Doctoral Research Fellow at Queen Mary University of London (QMUL). Since 2021, he has been an associate professor at BJTU. Dr. Hou's current research interests include next generation multiple access (NGMA), reconfigurable intelligent surface (RIS) aided communications, UAV communications, multiuser multiple-input multiple-output (MIMO) communications, and stochastic geometry. He has granted a Marie Sklodowska-Curie fellowship by European Research Executive Agency in 2023. He has been selected as a young elite scientist sponsorship program by China Association for Science and Technology in 2022. He received the Exemplary Reviewer of the IEEE COMMUNICATION LETTERS and the IEEE TRANSACTIONS ON COMMUNICATIONS in 2018, 2019 and 2022. He has served as a TPC Member for many IEEE conferences, such as GLOBECOM, VTC, etc. He served as the publicity officer for the Next Generation Multiple Access Emerging Technology Initiative (NGMA-ETI). He has served as a Co-Chair in the 2nd, 4th and 5th NGMA-for-future-wireless-communication workshops in IEEE VTC 2022-Fall, IEEE VTC 2023-spring, IEEE ISCT-2022 and IEEE PIMRC 2023. He has also served as a co-chair in the RIS and Smart Environments Symposium of IEEE ICCT 2023. He serves as the leading Guest Editor for IEEE IoT-J special issue on Next Generation Multiple Access for Internet of Things.

Da Guan received the B.S. degree in communication engineering from Beijing Jiaotong University (BJTU), China, in 2023, where he is currently pursuing Ph.D. degree.

His research interests include satellite integrated navigation and communication, RISs aided communication, and near-field sensing. He received the Best Paper Award at *IEEE International Conference on Information Systems and Computing Technology (ISCTech 2022)* in 2022.

Xin Sun received the Ph.D. degree in electromagnetic measurement technology and instrument from Harbin Institute of Technology, Harbin, China. She is currently a Professor with the School of Electronic and Information Engineering, Beijing Jiaotong University, Beijing, China. Her main research interests are professional mobile communications and wireless personal communications.

Anna Li received her Ph.D. degree in Computer Science from the School of Electronic Engineering and Computer Science, Queen Mary University of London, London, U.K., in 2023. She has been a Lecturer in the School of Computing and Communications at Lancaster University, Lancaster, U.K., since September 2023. She is also a Marie Curie Fellow at Katholieke Universiteit Leuven (KU Leuven), Leuven, Belgium. Her research expertise encompasses wireless sensing, satellite navigation and communication systems, signal processing, and deep learning.

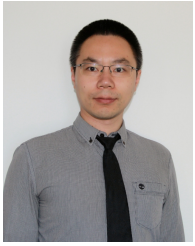

Wenqiang Yi (S'17-M'20) received his Ph.D. degree in electrical engineering from Queen Mary University of London, U.K., in 2020. He is currently an Assistant Professor in the School of Computer Science and Electronic Engineering, University of Essex, since 2023. From 2020 to 2023, he was a Post-Doctoral Researcher with Communication Systems Research Group, School of Electronic Engineering and Computer Science, Queen Mary University of London.

His research interests include AI in wireless communications, RF sensing, and stochastic geometry. He serves as an Associate Editor for IEEE OJ-COMS, in the area of Big Data and Machine Learning for Communications. He received the Exemplary Reviewer of the IEEE COMMUNICATION LETTERS and the IEEE TRANSACTIONS ON COMMUNICATIONS in 2019 and 2020. He served as the symposium chair on reconfigurable intelligent surfaces at IEEE ICCT. He has served as a TPC Member for many IEEE conferences, e.g., GLOBECOM and ICC.

Yuanwei Liu (Fellow, IEEE) received the Ph.D. degree from the Queen Mary University of London (QMUL), London, U.K., in 2016.

He is a tenured Full Professor with the Department of Electrical and Electronic Engineering (EEE), The University of Hong Kong (HKU); and a Visiting Professor with QMUL. Prior to that, he was a Senior Lecturer (an Associate Professor) (2021–2024) and a Lecturer (an Assistant Professor) (2017–2021) with QMUL; and a Post-Doctoral Research Fellow (2016–2017) with King's College London (KCL), London. His research interests include non-orthogonal multiple access, reconfigurable intelligent surface, near field communications, integrated sensing and communications, and machine learning. He is a fellow of AAIA; a Web of Science Highly Cited Researcher; an IEEE Communication Society Distinguished Lecturer; an IEEE Vehicular Technology Society Distinguished Lecturer; the Rapporteur of ETSI Industry Specification Group on Reconfigurable Intelligent Surfaces on work item of "Multi-Functional Reconfigurable Intelligent Surfaces (RIS): Modelling, Optimisation, and Operation;" and the U.K. Representative for the URSI Commission C on "Radio Communication Systems and Signal Processing." He was listed as one of 35 Innovators Under 35 China in 2022 by MIT Technology Review. He received the IEEE ComSoc Outstanding Young Researcher Award for EMEA in 2020, the 2020 IEEE Signal Processing and Computing for Communications (SPCC) Technical Committee Early Achievement Award, the IEEE Communication Theory Technical Committee (CTTC) 2021 Early Achievement Award, and the IEEE ComSoc Outstanding Nominee for Best Young Professionals Award in 2021. He was a co-recipient of the 2024 IEEE Communications Society Heinrich Hertz Award, the Best Student Paper Award in IEEE VTC2022-Fall, the Best Paper Award in ISWCS 2022, the 2022 IEEE SPCC-TC Best Paper Award, the 2023 IEEE ICCT Best Paper Award, and the 2023 IEEE ISAP Best Emerging Technologies Paper Award. He serves as the Publicity Co-Chair for IEEE VTC 2019-Fall; the Panel Co-Chair for IEEE WCNC 2024; and the Symposium Co-Chair for several flagship conferences, such as IEEE GLOBECOM, ICC, and VTC. He serves as the Academic Chair for the Next Generation Multiple Access Emerging Technology Initiative and the Vice Chair for SPCC and Technical Committee on Cognitive Networks (TCCN). He serves as the Co-Editor-in-Chief for IEEE ComSoc TC Newsletter; an Area Editor for IEEE TRANSACTIONS ON COMMUNICATIONS and IEEE COMMUNICATIONS LETTERS;an Editor for IEEE COMMUNICATIONS SURVEYS AND TUTORIALS,IEEE TRANSACTIONS ON WIRELESS COMMUNICATIONS,IEEE TRANSACTIONS ON VEHICULAR TECHNOLOGY,IEEE TRANSACTIONS ON NETWORK SCIENCE AND ENGINEERING,and IEEE TRANSACTIONS ON COGNITIVE COMMUNICATIONS AND NETWORKING. He serves as the (leading) Guest Editor for PROCEEDINGS OF THE IEEE on Next Generation Multiple Access, IEEE JOURNAL ON SELECTED AREAS IN COMMUNICATIONS on Next Generation Multiple Access, IEEE JOURNAL OF SELECTED TOPICS IN SIGNAL PROCESSING on Intelligent Signal Processing and Learning for Next Generation Multiple Access, and IEEE NETWORK on Next Generation Multiple Access for 6G. For more datails, please see https://www.eee.hku.hk/yuanwei/.

Arumugam Nallanathan (S'97-M'00-SM'05-F'17) is Professor of Wireless Communications and the Founding Head of the Communication Systems Re search (CSR) group in the School of Electronic Engineering and Computer Science at Queen Mary University of London since September 2017. He was with the Department of Informatics at King's College London from December 2007 to August 2017, where he was Professor of Wireless Commu nications from April 2013 to August 2017 and a Visiting Professor from September 2017 till August 2020. He was an Assistant Professor in the Department of Electrical and Computer Engineering, National University of Singapore from August 2000 to December 2007. His research interests include Artificial Intelligence for Wire less Systems, Beyond 5G Wireless Networks and Internet of Things (IoT). He published more than 700 technical papers in scientific journals and inter national conferences. He is a co-recipient of the Best Paper Awards presented at the IEEE International Conference on Communications 2016 (ICC'2016), IEEE Global Communications Conference 2017 (GLOBECOM'2017) and IEEE Vehicular Technology Conference 2018 (VTC'2018). He is also a co recipient of IEEE Communications Society Leonard G. Abraham Prize in 2022. He is an IEEE Distinguished Lecturer. He has been selected as a Web of Science Highly Cited Researcher in 2016, and 2022-2024.

He was a Senior Editor for IEEE Wireless Communications Letters, an Editor for IEEE Transactions on Wireless Communications, IEEE Transactions on Communications, IEEE Transactions on Vehicular Technology and IEEE Signal Processing Letters. He served as a Guest Editor for numerous special issues of IEEE Journal on Selected Areas in Communications (JSAC). He served as the Chair for the Signal Processing and Communication Electronics (SPCE) Technical Committee of IEEE Communications Society and Technical Program Chair and member of Technical Program Committees in numerous IEEE conferences. He received the IEEE Communications Society SPCE outstanding service award 2012 and IEEE Communications Society RCC outstanding service award 2014.